Journal Pre-proof

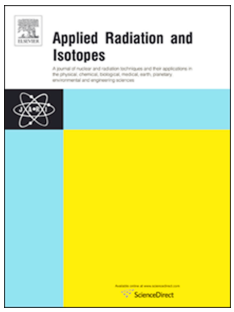

Dosimetry of tumor targeting imaging by convergent X-ray beam as compared with nuclear medicine

R. Figueroa, J. Guarda, J. Leiva, F. Malano, M. Valente

PII: S0969-8043(20)30595-9

DOI: https://doi.org/10.1016/j.apradiso.2020.109451

Reference: ARI 109451

To appear in: *Applied Radiation and Isotopes*

Received Date: 1 April 2020

Revised Date: 13 July 2020

Accepted Date: 24 September 2020

Please cite this article as: Figueroa, R., Guarda, J., Leiva, J., Malano, F., Valente, M., Dosimetry of tumor targeting imaging by convergent X-ray beam as compared with nuclear medicine, *Applied Radiation and Isotopes* (2020), doi: https://doi.org/10.1016/j.apradiso.2020.109451.

This is a PDF file of an article that has undergone enhancements after acceptance, such as the addition of a cover page and metadata, and formatting for readability, but it is not yet the definitive version of record. This version will undergo additional copyediting, typesetting and review before it is published in its final form, but we are providing this version to give early visibility of the article. Please note that, during the production process, errors may be discovered which could affect the content, and all legal disclaimers that apply to the journal pertain.

© 2020 Published by Elsevier Ltd.

Journal Pre-proof

Dosimetry of tumor targeting imaging by convergent X-ray beam as compared with nuclear medicine

R. Figueroa[1,2,*], J. Guarda[1,2], J. Leiva[1,2], F. Malano[1,2] and M. Valente[1,2,3,*]

[1] Centro de Física e Ingeniería Aplicada en Medicina (CFIM), Universidad de La Frontera, Temuco, Chile.
[2] Departamento de Ciencias Físicas, Universidad de la Frontera, Avda. Francisco Salazar, 01145 Temuco, Chile.
[3] Instituto de Física Enrique Gaviola (IFEG), CONICET & FAMAF – Laboratorio de Investigación e Instrumentación en Física Aplicada a la Medicina e Imágenes por Rayos X (LIIFAMIR^{X}), FAMAF - Universidad Nacional de Córdoba, Ciudad Universitaria, 5000, Córdoba, Argentina.

* Corresponding author: mauro.valente@gmail.com rodolfo.figueroa@ufrontera.cl

Abstract

During decades nuclear medicine procedures, based on radiolabeled agents, have proved to be efficient for diseases diagnosis and treatment. Radiation emerging from patient is detected aimed at localizing radiotracer distribution that is further correlated with biochemical/metabolic physiological processes. However, a significant drawback associated with current nuclear medicine procedures implementing radionuclide infusion regards to the inherent absorbed dose as well as radiopharmaceuticals' production, storage and elimination from patient body, thus representing a risk at patient and public health level.

In the recent years, alternative methods have been proposed to reduce/eliminate radionuclides in some nuclear medicine procedures. The combination of high atomic number nanoparticles infused within patient body with incident X-ray beam, like tumor targeting and treatment, appears as a potential alternative method capable of theranostics. The process is based on inducing X-ray fluorescence and secondary electrons emission in high atomic number nanoparticles by means of excitation with an external X-ray beam, avoiding employing radioactive substances.

The present work reports on the dosimetry performance of both methods, comparing whenever the external convergent X-ray beam alternative may involve less or larger radiation dose levels, according to comparable signal/image quality during the procedure. To this aim, a simplified theoretical model is proposed and associated Monte Carlo simulations are performed in order to compare typical case of nuclear medicine imaging with potential performance of an innovative method, called OXIRIS (Orthovoltage X-ray Induced Radiation and Integrated System), based on convergent X-ray beam exciting high atomic number nanoparticles infused in patient.

The obtained results support the proposed alternative method's feasibility, once demonstrated that patient absorbed dose levels are relative similar to those currently used by nuclear medicine procedures, whereas dose to targeted region (tumor) are significantly higher, which may be useful for treatment purposes.

Journal Pre-proof

Keywords: tumor targeting imaging; gold nanoparticle; convergent X-ray beam; Monte Carlo simulations.

1. Introduction

Nowadays, complex theranostics procedures stand as key issues in medical environment enabling functional/metabolic approaches to diagnose and therapy for a wide range of diseases [Yordanova et al. 2017; Saumya et al. 2019].

Nuclear medicine, mainly based on radiopharmaceuticals' uptake, represents one of the most commonly used medical procedures for metabolic physiology mapping [Carson 1991; Cherry 2004]. During the last decades, great efforts as well as active research were devoted to the study and application of molecular imaging to improve quality of functional imaging [Hainfeld et al. 2010; Ngwa et al. 2014] and also investigating radiolabeled molecules able to selectively target and irradiate tumor cells [Sofou 2008; Bavelaar et al. 2018].

Although these imaging modalities are capable of accurately assessing spatial distribution and corresponding activity of radiopharmaceuticals infused within the patient, there is the inherent undesired effect of employing ionizing radiations from radionuclides. Production, storage, management and even elimination of radioactive materials represent a drawback for standard nuclear medicine procedures. Moreover, radiation exposure risk for patient family and clinical staff is also a relevant issue for nuclear medicine.

In this context, alternative theranostics methods appear as promising options. The combination of high atomic number (Z) nanoparticles with external X-ray excitation has been proposed and preliminary explored as an alternative for tumor targeting and functional imaging [Figueroa et al. 2015; Hainfeld et al. 2013; Santibáñez et al. 2017]. One of the main advantages of such a technology relies on the absence of radioactive materials; radiation levels would be completely controlled during medical procedure, thus reducing irradiation, while avoiding unnecessary exposition of patient accompaniers and clinical staff.

In this regard, the OXIRIS (Orthovoltage X-ray Induced Radiation and Integrated System) project aims at developing and characterizing an integral system combining high Z nanoparticles infused within the patient with external convergent X-ray beam and confocal detection of induced emerging radiation. Briefly: high Z nanoparticles linked to appropriate carriers, like peptides [Kah et al. 2016; Porta et al. 2007], would selectively accumulate within patient's body, an external convergent X-ray beam, having a spot around 1mm side, excites X-ray fluorescence with high probability of leaving the patient to be suitably detected by a set of detectors confocally arranged.

However, characterization and comparisons between radiation dose levels involved in typical nuclear medicine procedures and those corresponding to alternative methods based on high Z nanoparticles

excited by external X-rays need to be properly established. The main purpose of the present work is to provide a simplified theoretical sketch to approach radiation dose levels in both cases, as well as modelling both cases by means of Monte Carlo simulations towards achieving more accurate approaches.

The obtained results highlight the feasibility of theranostics methods based on the combination of high *Z* nanoparticles excited by external X-ray and coupled with radiation detectors and are in fact a valuable alternative, or complement, to standard nuclear medicine procedures. Furthermore, the obtained results indicate that the corresponding radiation dose levels are comparable to those involved in typical nuclear medicine practices.

2. **Materials and Methods**

The dosimetry performance of the novel OXIRIS device was characterized by comparisons with a well-known theranostics clinical practice, as nuclear medicine procedures are. To this aim, two different approaches were implemented. Firstly, a dedicated analytical framework was developed and employed to get a preliminary estimation of absorbed doses; while more accurate assessments were obtained from Monte Carlo simulations.

2.1. **Theoretical model**

Figure 1 shows the simplified sketch representing the starting point for the theoretical overview about sample/patient imaging comparing traditional nuclear medicine technique with X-ray fluorescence detection due to high Z nanoparticle infusion in tumor-like regions and further excitation with external convergent X-ray beam. Also, it depicts the sample/patient (*P*) containing the tumor-like region (*T*) where radionuclides or high *Z* nanoparticle solution/suspension are infused. Detection of emerging radiation is performed by bi-dimensional X-ray detector (***D***), potentially coupled with suitable collimation grid, or a set of X-ray spectrometers (*S*) in the case of the OXIRIS device.

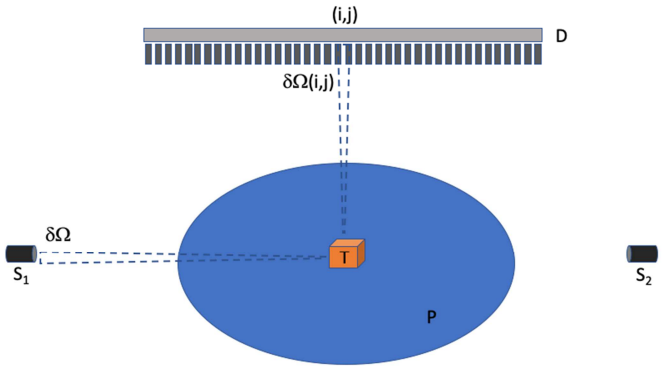

Journal Pre-proof

Figure 1: Simplified sketch highlighting relevant components for imaging by nuclear medicine and the OXIRIS device.

Assuming that the count rate at each pixel *(i,j)* of detector D is *dN/dt (i,j)* and its detection efficiency is characterized by $\varepsilon(E)$, according to the sketch in Figure 1, $\delta\Omega(i,j)$ represents the solid angle projected from emission point to the *(i,j)* detector pixel. As a simplified preliminary example, sample/patient is considered as 10 cm diameter water-equivalent sphere and tumor-like region is modelled as 1cm diameter concentric sphere infused with 1 % by weight of gold nanoparticles, thus constituting a uniform compound of gold (1 % w/w) and water (99 % w/w). Let's assume that $S_{0X.}(E)$ is the spectrum of the incident convergent X-ray beam and, similarly, $S_{N.M.}(E)$ is the emission spectrum from the radionuclide considered for the nuclear medicine imaging procedure.

As known, both the detection count rate and efficiency are key issues to attain similar comparable image/signal quality between the proposed method based on convergent X-ray beam excitation of high Z nanoparticle infusing tumor-like region and conventional nuclear medicine procedures. In this regard, the proposed principle for theoretical modelling of such methods is based on the following relation:

$$\left[\frac{dN}{dt}\right]_{N.M.} \cong \left[\frac{dN}{dt}\right]_{OX.} \wedge \quad \varepsilon(E)_{N.M.} \cong \varepsilon(E)_{OX.} \qquad (1)$$

where subscripts *N.M.* and *OX.* stand for nuclear medicine and the OXIRIS device; respectively.

2.1.1 **Modelling of convergent X-ray beam exciting high atomic number nanoparticles**

According to sketch in Figure 1, the convergent X-ray beam impacts on phantom surface with the spectrum $S_0(E)$, which is considered to be, for instance, a narrow Gaussian-like distribution centered at energy E_0.

Part of this incident spectrum $S_0(E)$ reaches the tumor-like region, and if scattering is neglected, as first approximation, the spectrum reaching the tumor-like region ($S_T(E)$) may be approximated by:

$$S_T(E) \approx S_0(E)\left[\left(e^{-\left(\frac{\mu}{\rho}\right)_W(E)\,\rho_W\,s_W}\right)\left(e^{-\left(\frac{\mu}{\rho}\right)_C(E)\,\rho_C\,s_C}\right)\right] \qquad (2)$$

where subscripts *W* and *C* refer to liquid water and compound made of high atomic number nanoparticles in water; respectively, *s* denotes the travelled path, ρ is the mass density and μ/ρ the total mass attenuation coefficient for the corresponding material.

Among those photons experiencing interactions at tumor-like region, the proportion interacting by photoelectric effect ($S_T^{Ph\text{-}E}(E)$) can be estimated as the photoelectric (τ/ρ_C) to total cross section (μ/ρ_C) ratio, thus:

$$S_T^{Ph-E}(E) \approx S_T(E) \cdot \frac{\left(\frac{\tau}{\rho}\right)_C(E)}{\left(\frac{\mu}{\rho}\right)_C(E)} \quad (3)$$

Besides, the probability fraction of producing characteristic X-ray K-lines due to photoelectric interaction in gold is around 95 % [Perkins et al. 1991], therefore the number of K fluorescent photons produced inside tumor-like region (I_K) can be approximated by:

$$I_K \approx I_0(E)\left[\left(e^{-\left(\frac{\mu}{\rho}\right)_W(E)\,\rho_W\,s_W}\right)\left(e^{-\left(\frac{\mu}{\rho}\right)_C(E)\,\rho_C\,s_C}\right)\right]\frac{\tau_{(E)}}{\mu_{Tot(E)}} \cdot 0.95 \quad (4)$$

where I_0 is the number of incident photons from the convergent X-ray beam entering the phantom surface. As known, fluorescent X-rays are emitted isotropically, therefore the number of photons emerging (leaving) the phantom (I_{exit}) can be estimated according to:

$$I_{exit} \approx 0.95\, I_0(E)\left[\left(e^{-\left(\frac{\mu}{\rho}\right)_W(E)\,\rho_W\,s_W}\right)\left(e^{-\left(\frac{\mu}{\rho}\right)_C(E)\,\rho_C\,s_C}\right)\right]\frac{\left(\frac{\tau}{\rho}\right)_C(E)}{\left(\frac{\mu}{\rho}\right)_C(E)} \cdot \left[\left(e^{-\left(\frac{\mu}{\rho}\right)_C(E_K)\,\rho_C\,s_C}\right)\left(e^{-\left(\frac{\mu}{\rho}\right)_W(E_K)\,\rho_W\,s_W}\right)\right] \quad (5)$$

where E_K is the energy of the characteristic K-line.

Once photons leave the phantom, only a limited portion actually reach the detection system (I_{det}). As described above, the fraction of detected photons can be estimated as solid angle ratio, *i.e.*: $\Delta\Omega_{det}/4\pi R^2$, where $\Delta\Omega_{det}$ is the solid angle corresponding to the whole detection system. Finally, photon rate reaching the detection system will be registered in terms of the corresponding detection efficiency $\varepsilon(E)$, hence:

$$\left[\frac{dN}{dt}\right]_{OX.} = \dot{I}_{det} \approx 0.95 \cdot \dot{I}_0(E)\left[\left(e^{-\left(\frac{\mu}{\rho}\right)_W(E)\,\rho_W\,s_W}\right)\left(e^{-\left(\frac{\mu}{\rho}\right)_C(E)\,\rho_C\,s_C}\right)\right]\frac{\tau\mu_{Tot(E)}}{\mu_{Tot(E)}} \cdot \left[\left(e^{-\left(\frac{\mu}{\rho}\right)_C(E_K)\,\rho_C\,s_C}\right)\left(e^{-\left(\frac{\mu}{\rho}\right)_W(E_K)\,\rho_W\,s_W}\right)\right] \cdot \frac{\Delta\Omega_{det}}{4\pi R^2} \cdot \varepsilon(E) =$$

$$0.95\varepsilon(E_K)\left[\left(e^{-\left[\left(\frac{\mu}{\rho}\right)_W(E)+\left(\frac{\mu}{\rho}\right)_W(E_K)\right]\rho_W\ s_W}\right)\left(e^{-\left[\left(\frac{\mu}{\rho}\right)_C(E)+\left(\frac{\mu}{\rho}\right)_C(E_K)\right]\rho_C\ s_C}\right)\right]\cdot \frac{\left(\frac{\tau}{\rho}\right)_C(E)}{\left(\frac{\mu}{\rho}\right)_C(E)}\cdot\frac{\Delta\Omega_{det}}{4\pi R^2}\cdot \dot{I}_0(E) \quad (6)$$

2.1.2 **Modelling of typical nuclear medicine imaging setup**

The proposed simplified approach, as used for the case of imaging by means of convergent X-ray beam exciting high *Z* nanoparticles, is depicted in Figure 1. A gamma-emitter radiotracer typically used in nuclear medicine imaging is quite uniformly distributed within the tumor-like region surrounded by concentric spherical water-equivalent phantom.

The detection system is supposed to be constituted of a typical square solid-state sensitive material coupled with a collimation grid. As previously proposed, in the convergent X-ray beam exciting high *Z* nanoparticles, it is considered that the detection system is close enough to the phantom. For practical purposes, different gamma-emitter radionuclides can be considered, as ^{99}Tc and ^{131}I, assuming only the main gamma decay branch is accounted. Initially, the activity A_0 is contemplated to be uniformly distributed within the tumor-like region. Therefore, the count rate of photons exiting the phantom ($(dN/dt)_{exit}$) can be approached as:

$$\left(\frac{dN}{dt}\right)_{exit} \approx \left[\left(e^{-\left(\frac{\mu}{\rho}\right)_c(E_\gamma)\,\rho_c\ s_c}\right)\left(e^{-\left(\frac{\mu}{\rho}\right)_W(E_\gamma)\,\rho_W\ s_W}\right)\right]\cdot A_0 \quad (7)$$

where E_γ is the energy of the main gamma line.

The collimation system's effect is modelled by means of a simplified analytical approach for the geometric efficiency G, defined as fraction of photons detected as those transmitted by collimator [Weinmann et al. 2009; Van Audenhaege et al. 2015], as follows:

$$G \equiv \frac{d^4}{12l^2(d+t)^2} \quad (8)$$

where d is the collimator hole size, t is the collimator septa thickness and l is the collimator length. Then, the detection count rate ($(dN/dt)_{det}$) can be approached by:

Journal Pre-proof

$$\left(\frac{dN}{dt}\right)_{det} \approx$$

$$A_0 \cdot \mathrm{G} \cdot \varepsilon(E_\gamma) \cdot \left[\left(e^{-\left(\frac{\mu}{\rho}\right)_c(E_\gamma)\,\rho_c\ s_c}\right)\left(e^{-\left(\frac{\mu}{\rho}\right)_W(E_\gamma)\,\rho_W\ s_W}\right)\right] \qquad (9)$$

It is worth noting that the approach proposed by equation (9) approximates source activity as being approximately constant during the imaging procedure lasting a few minutes.

2.2 **Monte Carlo simulations**

As known, radiation transport, including absorption and scattering processes, are described by the Boltzmann transport equation that is very hard to be applied in most practical cases, hence analytic solutions are commonly difficult when considering non-homogeneous media or regions consisting of complex boundaries. Therefore, numerical methods have been proposed for solving Boltzmann equation in complex situations performing full radiation transport by means of stochastic methods. The Monte Carlo techniques may be considered as the most representative of such approaches.

For the purposes of the present work, the PENELOPE v. 2014 Monte Carlo main code [Fernández-Varea et al. 2014] was implemented, for being suitable for radiation-matter interaction modelling within the energy range of interest, as well for its extended use in similar situations [Castellano et al. 2007, Santibañez et al. 2016, Valente et al. 2007, Pérez et al. 2018].

Dedicated subroutines were adapted to study typical setups for standard nuclear medicine procedures as well as OXIRIS configuration. Aiming to attain representative results, corresponding setups were simplified as much as possible, without compromising required level of realism.

Figure 2 depicts the setup consisting of a 10 cm diameter water-equivalent phantom including a concentric 1 cm diameter tumor region. Imaging system for nuclear medicine is considered as a 20 cm side square detector placed 10 cm from the phantom; whereas OXIRIS detection system consists of a set of four spectrometers (0.25 cm^2 active area) placed around the phantom and confocally disposed. To this aim, spectrometers are provided with 0.25 cm diameter and 2 cm long cylindrical collimators.

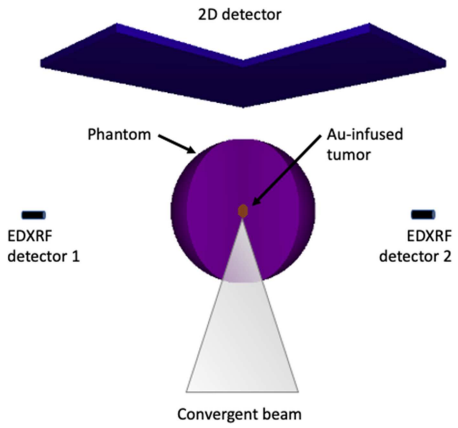

Figure 2: Geometry setup, as visualized by PENELOPE *gview* program, showing the tumor-like region composed of a solution made of 1 % w/w gold nanoparticles uniformly distributed in liquid water, the phantom consisting of 10 cm diameter water sphere, the bidimensional 400 cm^2 detector (multigrid collimation, made of too many bodies cannot be visualized by *gview*) , and two EDXRF detectors; along with a representation of the incident convergent beam, as proposed by OXIRIS.

Radiation-matter interactions properties for the different materials involved in the simulation were obtained as follows: PENELOPE v. 2014 provides a dedicated package with cross sections for pure elements and some compounds of typical use. Subsequently, liquid water and gold properties were directly obtained from PENELOPE database, as reported in Figure 3; whereas the mixture of 1% w/w gold in liquid water was user-defined by means of the *material* program distributed by the PENELOPE v. 2014 package allowing generating cross section data for arbitrary compound in terms of stoichiometry or fraction by weight of corresponding constituents.

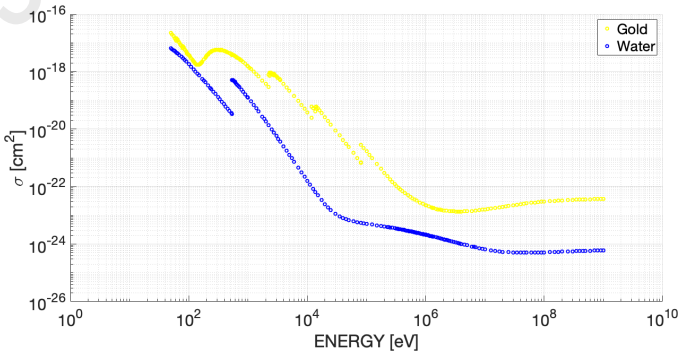

Figure 3: Total photon cross section for gold (yellow) and liquid water (blue), as provided by the PENELOPE v. 2014 code.

Mass density for the compound was estimated assuming uniform distribution of the nanoparticles in liquid water, thus constituting a uniform-like solution [Casanelli et al. 2020], whereas mass attenuation coefficient was assessed by means of the Bragg additivity rule in terms of constituents' fractions in

weight [Valente et al. 2018]; obtaining: $\rho_C \cong 1.183$ gcm^{-3} and $\mu/\rho_C \cong 0.01\mu/\rho_{NP} + 0.99\mu/\rho_W$, where subscript *NP* indicates high *Z* nanoparticles' material.

The convergent incident beam $S_{OX.}$, a key part of the OXIRIS device, was modelled, as first approximation, appearing to be perfectly convergent to the geometrical focus, thus producing the convergence spot at the center of the concentric spheres (gold nanoparticle infused tumor-like region and surrounding water phantom); whereas for more realism its spectrum was obtained from direct measurements of the X-ray source, which is currently part of the OXIRIS device, as reported in Figure 4. A solid-state CdTe Amptek XR123 spectrometer was used to measure photon spectra properly processed using the corresponding manufacturer provided software. Additionally, it is worth mentioning that a set of circular W collimators (diameters between 100 and 2000 microns) was employed to accurately assess the entering window area.

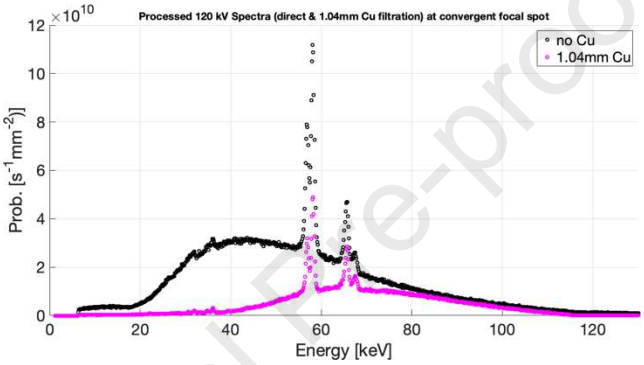

Figure 4: OXIRIS photon spectrum at focal spot with (magenta) and without (black) filtration.

The simulation was prepared to compute fluence of emerging particles from phantom surface. Similarly, calculations of spectra of photons reaching each one of the 4 simulated spectrometers (S_j, *j=1, 2, 3, 4*), aimed at operating as energy dispersive X-ray fluorescence (EDXRF), were undertaken along with the corresponding image at bi-dimensional detector for the typical nuclear medicine procedure. Multigrid collimation (1mm diameter septa) was placed directly before detection plane and the detector spatial resolution was set to 0.250mm, thus representing very good resolution parameters for typical nuclear medicine practice. ^{99m}Tc was used as radiopharmaceutical considering to be distributed as follows: 75 % of total decays (tumor-like uptake) are uniformly distributed within tumor-like region (1 cm diameter internal sphere), while 25 % of decays (background uptake) are uniformly distributed within the water-equivalent part of the spherical phantom.

The PENELOPE code provides absorbed energy in units of eV (E_{Abs}) for each body constituting the geometrical setup, then absorbed dose *D* is obtained as follows:

$$D\,[Gy] = \frac{1.60218 \cdot 10^{-19}\ J}{\frac{4\pi(r[m])^3}{3} \cdot 1.0 kg/m^3} \cdot E_{Abs}[eV] \qquad (10)$$

Journal Pre-proof

$$\rightarrow D_{Pha}[\mu Gy] \approx 3.06 \cdot 10^{-16}\ E_{Abs}[eV]$$
$$\rightarrow D_{Tum}[\mu Gy]\ \approx 3.06 \cdot 10^{-13}\ E_{Abs}[eV]$$

The corresponding uncertainties can be assessed considering the statistical deviations provided by PENELOPE along with error propagation of formula (10).

Finally, 20 mCi can be considered as a typical representative value of administered ^{99m}Tc activity for some customary nuclear medicine practices. For the OXIRIS device, a 100 mm^2 mapping area containing the tumor-like region was considered as the region of interest, assuming 1 mm of spatial resolution, *i.e.* requiring shifting/positioning 100 times. Total photon counts for the OXIRIS device can be suitably controlled by the applied current and irradiation time.

Simulations setup parameters were configured to transport charged particles by means of a mixed procedure, as recommended by PENELOPE manual. Simulation parameters for considering charged particle condensed simulation (W_{CC} and W_{CR}) were defined as recommended by PENELOPE manual; whereas cutoff values for absorption energy were set to 1 keV for all particles. This configuration led to total computation time in a typical desktop PC around 20 hours.

3. Results and discussions

*3.1. **Comparisons between simplified analytic approaches***

*3.1.1. **Simplified analytic approach to OXIRIS device***

Considering the analytic approach, the model assessment at 100 keV for the effective energy is intended as a representative approximation for an incident convergent spectrum. Then, taken numerical values for attenuation coefficients and cross sections from the NIST recognized database [NIST] and introducing the geometrical properties described in Figure 1, equation (6) can be evaluated, obtaining:

$$\left[\frac{\mathrm{dN}}{\mathrm{dt}}\right]_{\mathrm{OX.}} = \dot{I}_{det} \approx 8.3 \cdot 10^{-7} \cdot \dot{I}_0(100\ keV) \qquad (11)$$

Numerical results presented in equation (11) incorporates the approximation $\varepsilon(K_{\alpha 1} = 68.8\ keV) \approx 1$.

*3.1.2. **Simplified analytic approach to nuclear medicine device***

Evaluating equation (9) for ^{99m}Tc can be carried out using E_γ =142,7 keV as an approach for the multiple gamma ^{99m}Tc emission. Referring to geometrical arrangement described in Figure 1 and considering as practical example, typical values for collimation grid in nuclear medicine imaging practices, the parameters in formula (8) can be approached as: *d = 2 mm*, *t = 0.2 mm* and *l = 24 mm*, thus obtaining:

$$\left[\frac{\mathrm{dN}}{\mathrm{dt}}\right]_{\mathrm{N.M.}} = \left(\frac{dN}{dt}\right)_{det} \approx 2.6 \cdot 10^{-5} \cdot A_0 \qquad (12)$$

where $\varepsilon(E_\gamma(^{99m}Tc) = 142\ keV) \approx 1$ was taken as an acceptable approach, as considered for the previous case of the OXIRIS device.

Therefore, assuming a total amount of 20 mCi of ^{99m}Tc, as representative of typical clinical practice and supposing the photon fluence rate at focal spot, could be approximated as portion of the total counts above 100 keV obtained by experimental measurements and reported in Figure 4, the corresponding total photon counts during one second can be estimated as follows:

$$N_{OX.} \sim 8.3 \cdot 10^{-7} \cdot 10^{11} = 8.3 \cdot 10^{4} \qquad (13)$$

And

$$N_{N.M.} \sim 2.6 \cdot 10^{-5} \cdot (20 \cdot 3.7 \cdot 10^{7}) = 1.9 \cdot 10^{4} \qquad (14)$$

According to results obtained in expressions (13) and (14), the OXIRIS device may attain similar net photon counts reaching the detection system as a typical nuclear medicine imaging system.

3.2. Monte Carlo simulations

Figure 5 depicts an example of the image produced by the ^{99m}Tc in the bi-dimensional detector. As shown, a fairly high contrast can be appreciated among the tumor-like region and the water phantom.

Journal Pre-proof

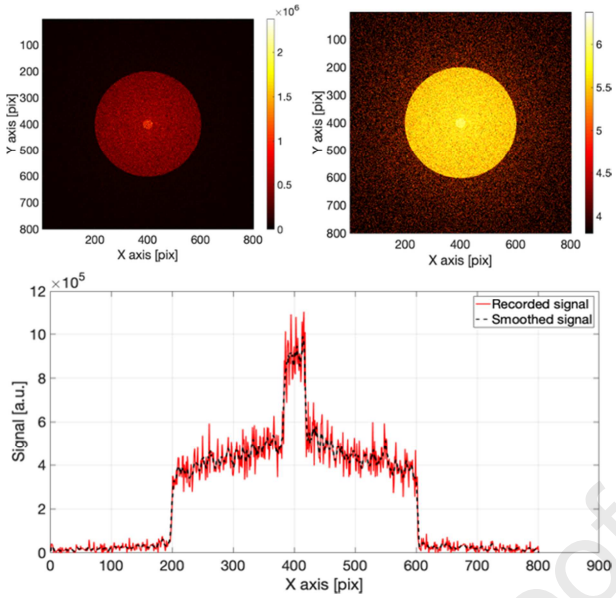

Figure 5: Image produced by ^{99m}Tc in linear (top left) and log (top right) scales along with central axis profile.

According to the signal profile, as taken at central axis, a signal-to-noise ratio around 2.5 is obtained for the detection of the tumor-like region in the acquired image. Successive planar projections at different angles may be used to reconstruct the tridimensional distribution of radionuclide (^{99m}Tc in this case), each one of those projections being analogue to the example reported in Figure 5.

Similarly, Figure 6 reports an example of typical net signal (difference between spectrum with and without Au infusion) as obtained by one of the four spectrometers employed by OXIRIS, thus remarking the capability for detecting the presence of gold by means of the K_α lines. It is worth mentioning that OXIRIS includes four spectrometers, hence the final signal is composed by combination of those four independent signals, which significantly improves the overall signal quality and associated uncertainty. Although the tumor-like region is placed in a 5 cm depth, the remarkable capacity of the convergent beam enables the detection system to record good enough signal quality to unequivocally distinguish the presence of gold nanoparticles, administered evenly in non-toxic concentrations. As may be appreciated, Figure 6 includes the incident spectrum, referred to a different scale, in order to emphasize that gold K_α line can be clearly distinguished of W K-lines coming from incident spectrum.

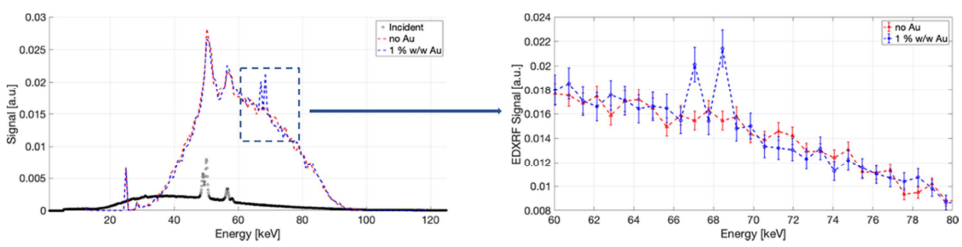

Figure 6: Net signal obtained by one of the spectrometers employed by OXIRIS corresponding to 1 % w/w gold nanoparticle infusion in 1 cm diameter tumor-like region surrounded by 10 cm diameter spherical water phantom. Channel corresponding to gold $K_{\alpha 1}$ (~69 keV) line is highlighted. Uncertainties are less than 7 % in all cases.

Additionally, it should be mentioned that when combining the four spectrometers to obtain the OXIRIS overall net signal, the signal-to-noise ratio for the $K_{\alpha 1}$ line is around 3.5, whereas it is 2.6 and 1.7 for $K_{\alpha 2}$ and K_{β} lines; respectively. Sequential point-by-point scanning of the region of interest may provide information enough to reconstruct the corresponding tri-dimensional distribution of gold nanoparticles, as the nuclear medicine practice does for the radionuclide distribution. Considering the focal spot position well-known by the OXIRIS device, the net signal (counts/s at K-lines' channels, subtracting background), as provided by the set of OXIRIS spectrometers, is used to construct the gold concentration mapping image, as illustrated in Figure 7.

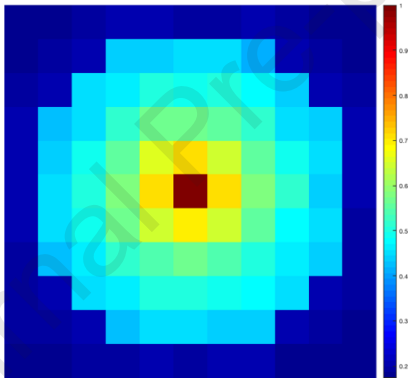

Figure 7: Example of gold nanoparticle spatial distribution, as reconstructed by the OXIRIS device using the $K_{\alpha 1}$ line.

Results summarized in Figures 5, 6 and 7; along with numerical values in expressions (13) and (14) demonstrate that both the standard nuclear medicine and the OXIRIS tumor imaging procedures are capable to provide reliable information employing a net quantity of “primary photons” equivalent to 20 mCi×s ($3.7\ 10^8$), however it remains necessary to estimate the corresponding dose levels. Therefore, the subroutine adapted from the PENELOPE Monte Carlo main code provided absorbed energy (per primary particle) E_{ABS} for each body constituting the simulation geometry. These values were converted to absorbed dose according to expression (10), obtaining the results summarized in Table 1.

Table 1: Absorbed dose for $3.7\ 10^8$ primary particles

Journal Pre-proof

BODY	$D_{N.M.}$ [μGy] = $\langle D_{N.M.} \rangle \pm \sigma_{D,N.M.}$	$D_{OX.}$ [μGy] = $\langle D_{OX.} \rangle \pm \sigma_{D,OX.}$
Phantom	(0.0021 ± 0.0002)	(0.0014 ± 0.0002)
Tumor	(0.33 ± 0.02)	(3.23 ± 0.09)

Phantom dimensions used as example for applying the theoretical and Monte Carlo approaches (10 cm diameter sphere containing 1 cm diameter spherical tumor) might not represent optimally all realistic clinical scenarios, specifically those corresponding to deep tumors. In fact, probability of emerging radiation would be decreased significantly for the OXIRIS device, due to the lower energy involved as compared with typical gamma radiotracers, as ^{99m}Tc. Nevertheless, the proposed approach is suitable for representing a wide variety of clinical cases. It is worth remarking that realistic in-patient dosimetry estimations for the nuclear medicine case should be significantly higher than those reported in Table 1, because the presence of an accumulated activity A_0 at certain target organ requires the administration of higher radiopharmaceutical activities. Moreover, contrary to the OXIRIS device, radiation distributed within the patient remains to be emitting even after medical practice, thus representing significant undesirable risks. Besides, the inherent properties of the OXIRIS technique have a noticeable impact on the absorbed dose at focal spot, which may be consequence of the Auger and secondary short-range electrons produced by the high atomic number nanoparticles. Therefore, this issue may provide the remarkable opportunity for the OXIRIS technique to combine tumor targeting and treatment simultaneously, thus constituting a promising system for threanostics. This capability is, of course, also available in nuclear medicine treatment procedures that may employ beta (or even alpha) emitters to attain high local dose concentration due to the radionuclide administration.

4. Conclusions

A novel simplified analytical approach has been proposed and implemented with the aim of providing a simple framework to characterize the dosimetry performance of imaging setups. The proposed model has been successfully implemented to analyze both a customary nuclear medicine practice and the non-conventional OXIRIS device, which is based on confocal detection of X-ray fluorescence from high atomic number nanoparticles infused in the patient and externally excited with a suitable X-ray convergent beam.

Journal Pre-proof

In addition, a more precise approach has been assessed by adapting dedicated Monte Carlo subroutines providing accurate information about emerging and detected photon spectra, image production by bi-dimensional detector, and absorbed dose for the different setup conditions. Tumor imaging practices have been characterized by image quality and corresponding absorbed doses have been evaluated in order to establish the feasibility of the OXIRIS technique when compared with a well-known method as routine nuclear medicine imaging.

Although accurate calculations should be performed in more complex situations involving anatomic geometry and actual materials/tissues, unlike regular shape and homogeneity, it is worth remarking that both the proposed simplified analytical model as well as the Monte Carto approach indicated that the OXIRIS device may represent similar dose levels as those typically accepted for daily nuclear medicine practices, thus preliminarily supporting the clinical feasibility of the innovative OXIRIS device.

Finally, it should be emphasized that the OXIRIS device does not require any radioactive substance, hence significant advantages can be expected for the patient, the health service, and general public.

Acknowledgments

This work has been supported by CONICYT program through FONDECYT project "*High energy EDXRF detection and excitation of targeting biomarkers by convergent beam: Physical characterization for novel detection tumor and radiotherapy techniques*" grant No. 1171729 and CFIM Universidad de La Frontera. Authors are grateful to Prof. Thomas "Rock" Mackie for his valuable suggestions about the relevance of assessing dosimetry performance comparisons between OXIRIS and standard nuclear medicine practices motivating and inducing the authors to undertake this significant research.

References

Bavelaar, B., Lee, B., Gill, M., Falzone, N., Vallis, K. (2018) Front. Pharmacol. 9, Art. 996

Carson, R. 1991. Journal of Cerebral Blood Flow & Metabolism. 11, A45-A50.

Casanelli, B, Santibáñez, M., Valente, M. (2020). Rad. Phys. Chem. 167,

Castellano, G. Brusa, D. Carrara, M. Gambarini, G., Valente, M. (2007). Nucl. Instrum. Meth. A 580, 502-505.

Cherry, S. 2004. Phys. Med. Biol. 49, R13–R48.

Fernández-Varea, J., Sempau, J. Salvat, F. (2014). NEA PENELOPE2014: A Code System for Monte-Carlo Simulation of Electron and Photon Transport

Figueroa, R., Santibañez, M., Valdez, C., Valente, M., 2015. Radiat. Phys. Chem. 117, 198-202.

Hainfeld, J., Dilmanian, F., Zhong, Z., Slatkin, D., Kalef-Ezra, J., Smilowitz, H., 2010. Phys. Med. Biol. 55, 3045-3059.

Hainfeld, J., Smilowitz, H., O'Connor, M.J., Dilmanian, F., Slatkin, D., 2013. Nanomedicine 8, 1601-1609.

Kah, S., Ma, L., Qiu, Y., Xun, X. Webster, T. Su, M. (2016). J. Biomed. Eng. 3, Art. 1003

Ngwa, W., Kumar, R., Sridhar, S., Korideck, H., Zygmanski, P., Cormack, R.A., Berbeco, R., Makrigiorgos, M., (2014). Nanomedicine 9, 1063-1082.

NIST database. https://www.nist.gov/

Pérez, P., Valente, M. (2018). Appl. Rad. Istop. 150, 135-140

Perkins S. et al. *Tables and graphs of atomic subshell and relaxation data derived from the LLNL evaluated atomic data library (EADL), Z = 1-100*, Report UCRL-50400 vol. 30 (Lawrence Livermore National Laboratory, Livermore, CA), 1991.

Porta, F., Speranza, G., Krpetića, Z., Dal Santo, V., Francescato, P., Scarìd, G. (2007). Mat. Sc. Eng. B, 140, 187-194.

Santibáñez, M., Saavedra, R., Vásquez, M., Malano, F., Pérez, P., Valente, M., Figueroa, R. 2017. Appl. Radiat. Isot. 129, 19-27.

Shrivastava Saumya, S., Saloni, J., Deepak, K., Shankar Lal, S., Mukesh. S. (2019). Asian Journal of Pharmaceutical Research and Development. 7, 63-69.

Sofou, S. (2008) Int. Jour. Nanomed. 3, 181-199.

Valente, M., Vedelago, J., Chacón, D., Mattea, F., Velásquez, J., Pérez, P. (2018). Appl. Rad. Isot., 141, 193-198.

Van Audenhaege et al. (2015). *Review of SPECT collimator selection, optimization, and fabrication for clinical and preclinical imaging*. Med. Phys. **42**, pp. 4796- 4813.

Weinmann et al. (2009). *Design of optimal collimation for dedicated molecular breast imaging systems*. Med. Phys. **36**, pp. 845-856.

Yordanova, A., Eppard, E., Kürpig, S., Bundschuh, R., Schönberger, S., Gonzalez-Carmona, M., Feldmann, G., Ahmadzadehfar, H., Essler, M. (2017). Onco Targets Ther., 10, 4821-4828.

Journal Pre-proof

Journal Pre-proof

Highlights

- A novel theranostic method based on convergent X ray beam and high Z nanoparticles is presented.
- Dosimetry performance of novel method is characterized by analytic and Monte Carlo approaches.
- The proposed method involves dose levels similar to typical nuclear medicine practices.

Journal Pre-proof

Journal Pre-proof

Author declaration

1. Conflict of Interest

Potential conflict of interest exists:

We wish to draw the attention of the Editor to the following facts, which may be considered as potential conflicts of interest, and to significant financial contributions to this work:

The nature of potential conflict of interest is described below:

X☐No conflict of interest exists.

We wish to confirm that there are no known conflicts of interest associated with this publication and there has been no significant financial support for this work that could have influenced its outcome.

2. Funding

X☐Funding was received for this work.

All of the sources of funding for the work described in this publication are acknowledged below:

☐No funding was received for this work.

3. Intellectual Property

X☐We confirm that we have given due consideration to the protection of intellectual property associated with this work and that there are no impediments to publication, including the timing of publication, with respect to intellectual property. In so doing we confirm that we have followed the regulations of our institutions concerning intellectual property.

Journal Pre-proof

Journal Pre-proof

4. Research Ethics

☐We further confirm that any aspect of the work covered in this manuscript that has involved human patients has been conducted with the ethical approval of all relevant bodies and that such approvals are acknowledged within the manuscript.

☐IRB approval was obtained (required for studies and series of 3 or more cases)

☐Written consent to publish potentially identifying information, such as details or the case and photographs, was obtained from the patient(s) or their legal guardian(s).

X☐ Not applicable

5. Authorship

1. Substantial contributions to the conception or design of the work: M.V. and R.F.
2. Monte Carlo simulations, data processing, and analysis for the work: M.V. F.M. J.G.
3. Experimental measurements and processing: J.G. J.L. R.F. and M.V.
4. Drafting the work or revising it critically for important intellectual content: M.V.
5. Final approval of the version to be published: M.V. and R.F.
6. Agreement to be accountable for all aspects of the work in ensuring that questions related to the accuracy or integrity of any part of the work are appropriately investigated and resolved: M. V. and R.F.

X☐We confirm that the manuscript has been read and approved by all named authors.

X☐We confirm that the order of authors listed in the manuscript has been approved by all named authors.

Journal Pre-proof

Journal Pre-proof

Declaration of interests

☒ The authors declare that they have no known competing financial interests or personal relationships that could have appeared to influence the work reported in this paper.

☐The authors declare the following financial interests/personal relationships which may be considered as potential competing interests:

Journal Pre-proof